European Journal of Radiology 112 (2019) 59–64

Contents lists available at ScienceDirect

European Journal of Radiology

journal homepage: www.elsevier.com/locate/ejrad

Research article

Differentiation of primary central nervous system lymphoma from high-grade glioma and brain metastasis using arterial spin labeling and dynamic contrast-enhanced magnetic resonance imaging

Yi-bin Xi[a,1], Xiao-wei Kang[a,1], Ning Wang[a], Ting-ting Liu[a], Yuan-qiang Zhu[a], Guang Cheng[b], Kai Wang[b], Chen Li[a], Fan Guo[a,c,*], Hong Yin[a,*]

[a] Department of Radiology, Xijing Hospital, The Fourth Military Medical University, Xi'an, 710032, China
[b] Department of Neurosurgery, Xijing Institute of Clinical Neuroscience, Xijing Hospital, Fourth Military Medical University, Xi'an, 710032, China
[c] Key Laboratory of Molecular Imaging of the Chinese Academy of Sciences, Institute of Automation, Chinese Academy of Sciences, Beijing, 100190, China

ARTICLE INFO

Keywords:
Primary central nervous system lymphoma
High-grade glioma
Metastasis
Arterial spin labeling
Dynamic contrast-enhanced perfusion

ABSTRACT

Background and purpose: Conventional magnetic resonance imaging (MRI) is sometimes difficult to distinguish primary central nervous system lymphoma (PCNSL) from other malignant brain tumors effectively. The study aimed to evaluate the diagnostic performance of arterial spin labeling (ASL) and dynamic contrast-enhanced (DCE)-derived permeability parameters to differentiate PCNSL from high-grade glioma (HGG) and brain metastasis.

Materials and methods: Eight patients with PCNSL, twenty one patients with HGG and six brain metastasis underwent preoperative 3.0-T MR imaging including conventional, ASL and DCE. Quantitative parameters including relative cerebral blood flow (rCBF), extravascular extracellular volume fraction (V_e) and the volume transfer constant (K^{trans}) among PCNSL, HGG and metastasis were compared with a one-way analysis of variance. In addition, the area under the receiver-operating characteristic (ROC) curve (AUC) was constructed to evaluate the differentiation diagnostic performance of each parameter and the combination.

Results: The PCNSL demonstrated significantly lower rCBF, higher K^{trans} and V_e compared with HGG and metastasis. For the ROC analyses, both K^{trans} and rCBF had good diagnostic performance for discriminating PCNSL from HGG and metastasis, with the AUC of 0.880 and 0.889. With the combination of rCBF and K^{trans}, the diagnostic ability for PCNSL was improved with AUC of 0.986.

Conclusion: rCBF and K^{trans} are useful parameters for differentiating PCNSL from HGG and brain metastasis. The combination of rCBF and K^{trans} further helps to improve the diagnostic performance of PCNSL.

1. Introduction

Primary central nervous system lymphomas (PCNSL) account for 3–5% of all primary brain tumors [1]. The differentiation of PCNSL, high-grade glioma (HGG) and brain metastasis could be sometimes challenging with conventional magnetic resonance imaging (MRI) although PCNSL demonstrate some characteristic MRI findings [2]. Atypical features such as necrosis, hemorrhage or heterogeneous enhancement in PCNSL could make it more difficult to diagnose [3]. Diagnose of PCNSL is clinically important, as the clinical outcomes and treatment for those three tumors are completely different [4].

PCNSL, HGG and metastasis are different histologically. The PCNSL generally shows little neovascularization but increased vascular permeability due to the architectural distortion of the vessels, whereas neovascularization and vascular permeability varies in HGG and metastasis [5]. Previous published data indicate that advanced imaging techniques could help to distinguish PCNSL, HGG and metastasis such as diffusion-weighted, susceptibility weighted, and dynamic susceptibility contrast-enhanced perfusion-weighted imaging [2,4,6]. They could provide some information not provided by conventional MRI.

Arterial spin labeling (ASL), a perfusion imaging technique that utilizes electromagnetically labeled arterial blood water as an intrinsic tracer, could be used to assess cerebral blood flow (CBF) in tumor. Dynamic contrast-enhanced magnetic resonance imaging (DCE-MRI) is a useful MR perfusion imaging technique. It could reflect quantitively for vascular microenvironment by measuring several permeability

* Corresponding authors at: No. 127 Changle West Road, Xi'an, Shaanxi, 710032, China.
E-mail addresses: guofan@fmmu.edu.cn (F. Guo), yinhong@fmmu.edu.cn (H. Yin).
[1] These authors contributed equally to this work.

https://doi.org/10.1016/j.ejrad.2019.01.008
Received 17 August 2018; Received in revised form 2 December 2018; Accepted 7 January 2019
0720-048X/

parameters such as the volume transfer constant (K^{trans}) and the fractional volume of the extravascular and extracellular space (V_e) [7]. Those two methods have been used for glioma grading and predicting therapeutic response or prognosis [8–10]. Prior studies also have successfully characterized PCNSL, glioma and brain metastasis with DCE-MRI [5,11]. Therefore, the combination of ASL and DCE-MRI is promising to reflect the nature of PCNSL and has the potential to increase the accuracy for discrimination from PCNSL to HGG and metastasis. To our knowledge, only few studies have focused on the clinical utility of ASL and DCE to differentiate HGG, brain metastasis and PCNSL [12,13].

The aim of this study was to compare ASL perfusion and DCE-MR imaging-derived permeability parameters to assess the diagnostic performance for differentiation of PCNSL from HGG and metastasis.

2. Materials and methods

2.1. Subjects

Our institutional review board approved this retrospective study, and the requirement for informed consent was obtained from all of the patients. From January 2015 to December 2017, thirty five patients with histologically confirmed HGG, PCNSL and metastasis were reviewed. All the tumors were confirmed by histopathological examination after surgical resection or biopsy and classified according to the new WHO Classification of Tumors of the Central Nervous System. All of the patients underwent conventional MRI, ASL and DCE MRI preoperatively. Finally, twenty one HGG (12 men, 9 women, mean age 54 years, range 32–80 years), eight PCNSL (5 men, 3 women, mean age 60.5 years, range 42–82 years) and six metastasis (3 men, 3 women, mean age 50 years, range 42–57 years) were enrolled. The patients' histological types of gliomas were as follows: two anaplastic astrocytoma (NOS), three oligodendrogliomas (IDH-mutant and 1p/19q-codeleted), and sixteen glioblastoma (GBM, NOS). Pathologically, all of the PCNSL in our study were diffuse large B-cell lymphomas. We excluded PCNSL patients with (1) systemic lymphoma, (2) non-parenchymal PCNSL, (3) those who had received therapy prior to PCNSL diagnosis, and (4) known history of testing positive for human immunodeficiency virus. In the 6 patients with brain metastases, the primary sites of the tumors were lung (n = 4), gastric (n = 1) and cervical cancer (n = 1).

2.2. MR imaging acquisition

An 8-channel head-matrix coil obtained MRI images on a 3.0 T MR System (Discovery MR750, GE Healthcare, Milwaukee, Wisconsin, USA). Our conventional MRI protocol included the following sequences: axial T1WI (TR, 1750 ms; TE, 24 ms; section thickness, 4 mm; inter-slice gap = 0 mm; field of view (FOV), 240 × 240 mm^2; matrix, 320 × 256); T2WI (TR, 3976 ms; TE, 92 ms; section thickness, 5 mm; inter-slice gap = 1.5 mm; FOV, 240 × 240 mm^2; matrix size, 512 × 512); FLAIR (TR, 8400 ms; TE, 145 ms; section thickness, 5 mm; inter-slice gap = 1.5 mm; FOV, 240 × 240 mm^2; Matrix size, 160 × 256); and DWI (TR, 3300 ms; TE, 65.8 ms; matrix, 256 × 256; slice thickness, 5 mm; FOV, 240 × 240 mm^2; scan time, 26 s; b values, 0 and 1000sec/mm^2).

The ASL perfusion imaging was performed using a pseudo-continuous ASL pulse sequence. ASL images were acquired with a background-suppressed 3-dimensional gradient and spin echo single-shot readout (TR, 4632 ms; TE, 10.5 ms; section thickness, 4 mm; inter-slice gap = 1.5 mm; FOV, 240 × 240 mm^2; spatial resolution, 3.64 mm; in-plane matrix, 128 × 128, bandwidth = 62.6 kHz; number of slices = 36; number of excitations, 3; acquisition time, 4 min 27 s).

Axial DCE MR imaging was performed with volume interpolated gradient echo (VIBE) sequence. Firstly, five non-enhanced datasets were acquired using T1WI VIBE (TR, 4.1 ms, TE, 2.0 ms, slice thickness, 4 mm, FOV, 240 mm^2, matrix, 256 × 192) with flip angles of 3°, 6°, 12° and 15° respectively to obtain the T1 map. Secondly, the dynamic sequence started after five baseline acquisitions. An intravenous injection of 0.2 mmol/kg gadodiamide (Omniscan, GE Healthcare, Ireland) was carried out at an injection rate of 4 ml/s via a power injector, followed by a flush of 20 mL of normal saline. The parameters were as follows: TR 4.1 ms, TE 2.0 ms, slice thickness 4 mm, FOV 240 mm^2, Matrix 256 × 192, flip angle 15°. Fifty dynamic phases were obtained in total and the temporal resolution was 7 s. Another contrast-enhanced T1WI was acquired after the completion of DCE MR imaging.

2.3. Image processing and analysis

Two neuroradiologists with 10 years of experience who were blinded to the diagnosis analyzed lesion number, enhancing pattern, hemorrhage and necrosis. The enhancing patterns were classified into two types: (1) homogeneous pattern: well-defined nodular lesions without hemorrhagic components or necrosis and homogeneously enhanced; (2) heterogeneous pattern: lesions with a presence of hemorrhage and/or necrosis and heterogeneous enhancement [3]. The two readers made final decisions by consensus. In cases of disagreement, a senior neuroradiologist with 20 years of experience helped to make the final decision.

The data were transferred to an off-line workstation for post-processing (Advantage Workstation, AW4.5; GE Medical Systems; Omini-Kinetics, Version V. 2.08) supplied by the vendor and respectively post-processed CBF maps and DCE maps using GE FuncTool software. To define the tumor localization and extension, the T1 post-contrast was used. These images were then assigned to coregistered Pulsed ASL (PASL) images. To approximate the whole tumor volume, tumor regions of interest (ROI) were manually drawn, at two continuous imaging slices, by an experienced neuroradiologist who was blinded to the tumor histopathology. Areas with necrosiswas attempted to be spared. The mean signal intensity value of each slice of one tumor was used to calculate the average mean signal intensity of the tumor regions of interest. A ROI of equal size was positioned at each slice exactly in the contralateral healthy hemisphere to calculate the average mean signal intensity of the contralateral normal brain tissue. In addition, we calculated the relative CBF values (rCBF) by normalizing to the contralateral normal-appearing gray matter.

Preprocessing of perfusion data included noise correction and motion rectification. For the purpose of the vascular input function (VIF), a ROI was placed in the superior sagittal sinus according to the previous report. The VIF curve was approved by a senior neuroradiologist to ensure its accuracy. The modified Tofts model was used to calculate pharmacokinetic parameter maps, including K^{trans} and V_e maps. ROIs encompassing the entire contrast-enhancing tumor were manually drawn from the DCE images of the last dynamic phase without necrosis and then transferred to the matching parametric maps (K^{trans}, V_e maps) to obtain the average mean value of the pharmacokinetic parameters.

2.4. Statistical analysis

All values are expressed as mean ± standard deviation (SD). Interobserver agreement for the tumor CBF, K^{trans} and V_e values from the 2 readers was analyzed by calculation of the intraclass correlation coefficient (ICC). ICCs are considered to be excellent if greater than 0.74 [14]. The measurements by the two observers for each patient were averaged for further analysis. Demographic information was analyzed using student's *t*-test and Fisher's exact test. One-way analysis of variance (ANOVA) test was used to compare the CBF, rCBF K^{trans} and V_e values among HGG, PCNSL and metastasis. When statistical differences existed, the post-hoc test was further performed using Dunnett tests treating PCNSL as the control and comparing all other groups against it. To minimize inter-individual differences in perfusion, signal intensities of intratumoral ROIs for each subject were normalized by dividing the values by those of contralateral normal gray matter (cCBF). Using the permeability parameters with rCBF and K^{trans} values, a

Table 1
Clinical characteristics of patients.

	PCNSL (n = 8)	HGG (n = 21)	Brain metastasis (n = 6)
Age (years)	60.5	54.0	50.0
Sex (male: female)	5: 3	12: 9	3: 3
Number of lesions			
Single lesion	5	14	1
Multiple lesions	3	7	5
Enhancing pattern			
Homogeneous	4	0	0
Heterogeneous	4	21	6
Necrosis	3	21	6
Hemorrhage	1	8	0

multivariate logistic regression model was built. The area under the curve (AUC) from receiver operating characteristic (ROC) analysis was used to evaluate the diagnostic performance of the ASL-determined CBF and DCE determined K^{trans} for differentiating the three brain tumors. In addition, cross-validated AUC was performed with a leave-oneout method to prevent overfitting. Statistical analyses were performed with SPSS (SPSS v. 19.0, Chicago, IL) and GraphPad Prism (GraphPad Prism v. 5.0, San Diego, CA). *P* values of less than 0.05 were considered to be statistically significant.

3. Results

3.1. Patients demographics and conventional MRI features

The clinical characteristics of subjects were summarized in Table 1. There was no statistical difference in male-to-female ratio or age between the three groups. The conventional MRI manifestations are also summarized. The representative MRI of a patient with PCNSL, HGG or metastasis was shown in Fig. 1. Several atypical features were observed in PCNSL: heterogeneous enhancement and necrosis, without elevated diffusion-weighted signal, as shown in Fig. 3.

3.2. Differences in CBF, K^{trans} and V_e among PCNSL, HGG and metastasis

Supplementary Table 1 shows the ICCs of the measurements by the two observers. Excellent agreement was observed for CBF, K^{trans} and V_e values.

Absolute CBF, as well as rCBF, was significantly lower in the patients with PCNSL than in those with HGG or metastasis. The K^{trans} and V_e values of PCNSL were significantly higher than those of HGG and metastasis. Detailed differences of quantitative analyses were summarized in Table 2 and Supplementary Table 2 and representative ASL and DCE images were shown in Fig. 1.

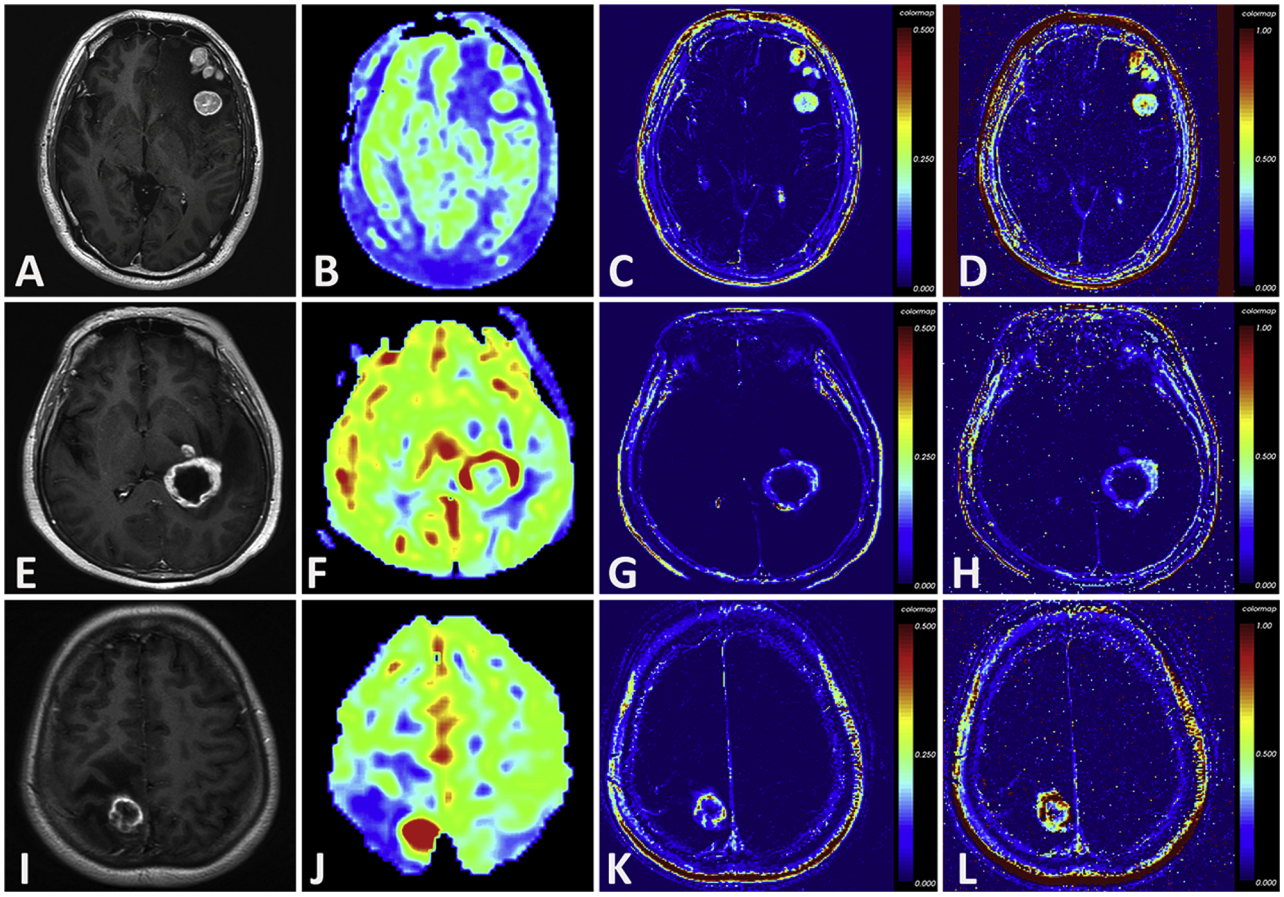

Fig. 1. Comparison among PCNSL (A–D), HGG (E–H) and metastasis (I–L). Upper row: A 43-year-old male with PCNSL in the left frontal lobe shows remarkable enhancement on a contrast-enhanced T1-weighted image (A). The matching ASL map shows iso-perfusion in the region of tumor compared with the contralateral brain. K^{trans} map (C) and V_e (D) shows obviously elevated signals in the enhancing region of the tumor, respectively. Middle row: A 49-year-old female patient with GBM beside the left posterior lateral ventricle shows irregular enhancement on a contrast-enhanced T1-weighted image (E). ASL perfusion map shows hyperperfusion in the mass compared with the contralateral brain (F). The K^{trans} (G) and V_e map (H) shows increased signals to the normal brain tissue, but significantly lower than those in PCNSL. Lower row: A 42-year-old female with metastatic tumor in the right parietal lobe with irregular and peripheral enhancement (I). ASL map shows hyperperfusion in the mass (*J*). On K^{trans} map (K) and V_e map (L), the signals are lower than those in PCNSL. Absolute color scheme is used to generate the color maps.

Table 2
DCE and ASL imaging-derived parameters for PCNSL, HGG and metastasis.

	PCNSL (n = 8)	HGG (n = 21)	Brain metastasis (n = 6)	P values
CBF	42.78 ± 7.48	96.60 ± 44.17	81.98 ± 32.13	0.0065
rCBF	0.99 ± 0.11	2.01 ± 0.81	1.72 ± 0.77	0.0068
K^{trans} (min^{-1})	0.50 ± 0.18	0.25 ± 0.08	0.29 ± 0.10	< 0.001
V_e	0.83 ± 0.19	0.68 ± 0.25	0.47 ± 0.31	0.0469

P value represents the comparison results of all the HGG, PCNSL and metastasis using the one-way analysis of variance analyzation. Values are presented as Mean ± standard deviations. rCBF = relative cerebral blood flow.

Table 3
Diagnostic performance of rCBF, K^{trans} and the combinations for differentiating PCNSL from HGG and metastatic tumors.

Model	AUC	Cutoff value	Sensitivity	Specificity	Cross-validated AUC
rCBF	0.880 (0.765-0.995)	1.202	0.815	1.000	0.879
K^{trans}	0.889 (0.736-1.000)	0.429	0.750	0.963	0.890
Multivariate	0.986 (0.954-1.000)	0.631	0.889	1.000	0.984

Data in parentheses are 95% confidence intervals. AUC = area under the receiver operating characteristic curve. rCBF = relative cerebral blood flow.

3.3. Diagnostic values of rCBF and K^{trans} alone and in combination

The ROC analysis for rCBF showed an AUC of 0.880 with a sensitivity of 81.5% and a specificity of 100%. According to the ROC curve analyses, the AUC of K^{trans} was 0.889 with a sensitivity of 75% and a specificity of 96.3%. Moreover, combination of rCBF and K^{trans} predicted PCNSL showed an AUC of 0.986 with a specificity of 100% and sensitivity of 88.9%. The optimal cutoff values of different parameters for discriminating PCNSL from HGG and metastasis were summarized in Table 3. The ROC curves are shown in Fig. 2.

4. Discussion

In the present study, PCNSL exhibited lower CBF values based on ASL perfusion MRI. PCNSL were also differentiated from HGG and metastatic tumors with significant elevated K^{trans} and V_e derived from DCE MR imaging. Moreover, with the combination of rCBF and K^{trans} value, the diagnostic performance was significantly improved for differentiating PCNSL from HGG and metastasis.

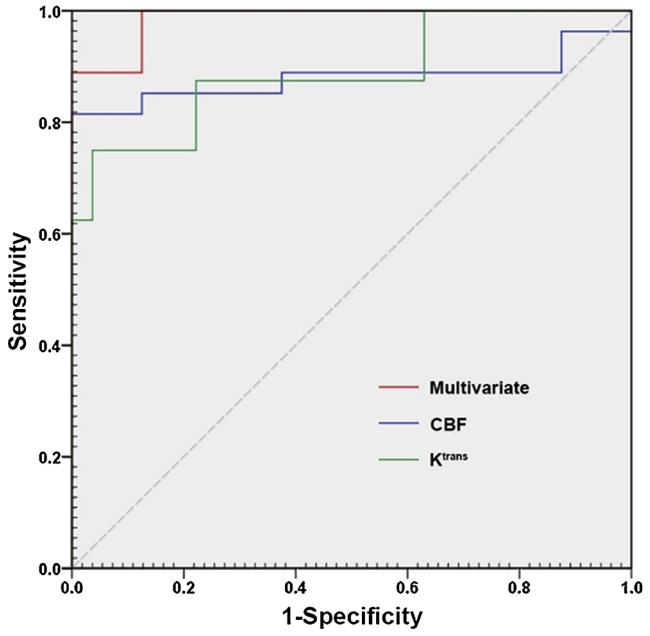

Fig. 2. Receiver operating characteristic curves for rCBF, K^{trans} and a combination of rCBF and K^{trans} for differentiating PCNSL from HGG and metastasis. AUC = area under the receiver operating characteristic curve. rCBF = relative cerebral blood flow.

Differentiation of PCNSL, HGG and metastasis is important as the therapeutic approach and prognosis are different clinically. HGG, especially GBM, is usually a ring-shaped contrast-enhanced mass lesion with central hypointense necrosis on contrast-enhanced T1-weighted MR imaging, whereas PCNSL usually present as a solid mass lesion with homogeneous contrast enhancement in immunocompetent patients [15]. Meanwhile, in patients with known primary malignancy or multiple brain lesions, the diagnosis of brain metastasis is without much difficulty. However, certain typical pattern is not always reliable as atypical features may mimic each other (Fig. 3), and without certain clinical history, differentiation of brain metastasis from other brain tumors becoming challenging with overlapping imaging features. Therefore, differential diagnose is sometimes difficult among PCNSL, HGG and metastasis.

In the current study, we firstly focused on the utility of intratumoral perfusion from ASL. PASL measurements, using low inversion times, could reflect only arterial vessels without affected by blood products, necrosis or calcification [1]. We found lower rCBF in PCNSL compared with HGG and metastasis, which was in agreement with previous studies [16,17]. Noguchi et al. have proposed that ASL-driven CBF may predict histopathologic vascular densities of brain tumors [18]. Therefore, our result may be attributed to that both HGG and metastatic brain tumors could induce angiogenesis, which lead to increased perfusion, but the angiogenesis is rare in PCNSL.

Second, we used DCE-derived parameters for the differentiation diagnose. Compared to dynamic susceptibility contrast-enhanced imaging, DCE perfusion has the advantages of higher spatial resolution, better quantification of microvascular leakiness and perfusion, and increased resistance to susceptibility artifacts [19]. We observed higher K^{trans} and V_e in PCNSL compared with HGG and metastasis. K^{trans} is the volume transfer constant of the gadolinium agent between the blood plasma and the extracellular extravascular space (EES), which could reflect tissue leakiness [20]. PCNSL has a greater degree of blood-brain barrier (BBB) disruption and thus a higher vascular permeability as compared to HGG and metastasis. Warnke et al. compared the vascular permeability between PCNSL and GBM and reported higher K^{trans} in PCNSL [21]. Kickingereder et al. studied the DCE-MR imaging-derived vascular permeability parameters for differentiation of PCNSL and GBM. And they also observed higher K^{trans} in PCNSL [5].

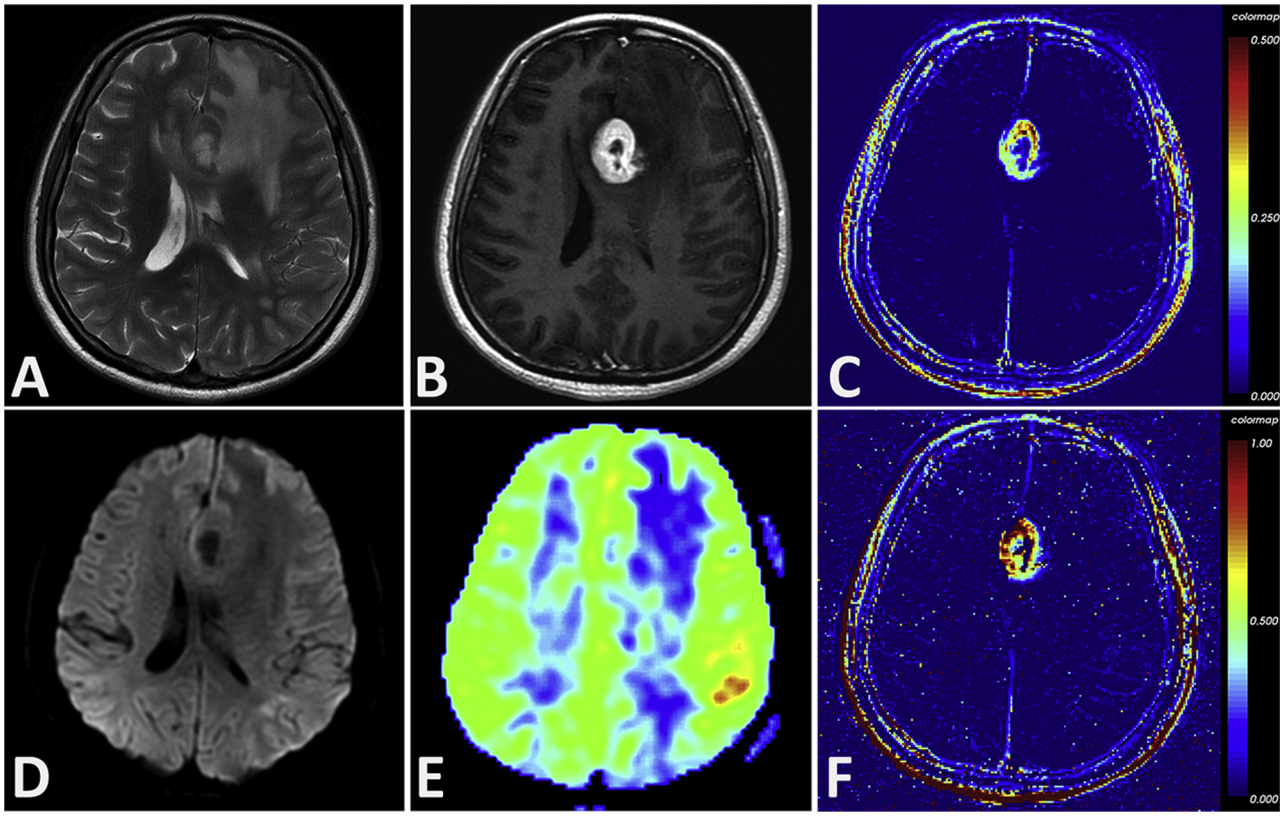

Fig. 3. A 42-year-old female with PCNSL. A, Axial T2WI shows a mass located in the frontal lobe, with edema. B, Axial contrast-enhanced T1WI shows the mass with necrosis and heterogeneous enhancement. C and F show the corresponding K^{trans} map (C) and V_e map (F), demonstrating obviously elevated signals in the tumor. D, the mass appears without hyperintensity on diffusion-weighted imaging. E, no hyperintensity on the ASL map in the region of the tumor could be detected.

Pathologically, they found the outer border of the vessel wall in PCNSL was infiltrated by tumor cells and destroyed, while the basal membrane of vessels in GBM was intact. Moreover, thinner endothelial cells, as well as the absence of endothelium between the vascular lumen and basement membrane has been reported in PCNSL [22]. These pathological findings confirm a large disruption of BBB in PCNSL, thus giving rise to higher K^{trans} value in our study. However, there are some controversial results from other studies. Lin et al. indicated that K^{trans} showed no difference between GBM and PCNSL [23]. The result might be attributed to the use of different model for calculation the parameters. In addition, V_e is defined as the volume fraction of contrast agent transferring from the vessel into the EES. The higher Ve value was related to the dose of the contrast agent in the tumor interstitium. Johnson et al. reported the V_e of PCNSL was higher than that of HGG [24], which was in agreement with our study. Recently, Abe et al. also observed that PCNSL had an extremely high V_e [12]. In Lu et al.'s study, higher V_e was observed in PCNSL than in GBM and metastasis as well [3].

On the other hand, our study showed that no differences were observed between PCNSL and metastasis in CBF and K^{trans} with post-hoc analysis in supplementary materials. Our result also indicated no differences between HGG and metastasis in those three parameters. Previous study proved that ASL perfusion MRI could aid in the differentiation of GBM from brain metastasis [25]. The possible explanation for the controversial result may due to the limited patients number for PCNSL and metastasis groups in our study. The difference of vascular permeability between HGG and brain metastasis in previous reports also stands out to be controversial. Server et al. found higher microvascular leakage in GBMs than in brain metastasis [26]. In contrast, Zhao et al. found higher K^{trans} in metastasis than in GBM, whereas Weber et al. found no significant difference between GBMs and metastasis [27]. Lüdemann et al. also reported that the permeability of metastasis was similar to that of gliomas [28]. We consider that the permeability parameters in brain metastasis might be greatly influenced by the histopathology of the primary tumors, therefore contributing to their results.

Most importantly, we proved that the combination of rCBF and K^{trans} values could significantly improve diagnostic performance in differentiating PCNSL from HGG and metastasis. Although some other methods may offer high accuracy with up to 90% for the differentiation diagnose, the evaluation is rather single parameters and could only reflect one characteristic for the brain tumors [2,4,6]. Moreover, previous study proved that multiple parameters could offer higher sensitivity and specificity [29]. Choi et al. proved that initial AUC derived from DCE-MRI and ADC could be useful for differentiating between the PCNSL and atypical GBM [30]. And Lu et al. proved that the combination of ADC and K^{trans} helps to improve the diagnostic accuracy [7]. Bauer et al. have shown that the combination of diffusion and perfusion matrices in non-enhancing peritumoral T2 hperintense region could help differentiate GBM over solitary brain metastasis [31]. With the combination of those parameters from DCE and ASL, the vascular densities as well as the vascular permeability and leakage were reflected at the same time. In our study, ASL and DCE showed somehow different trends in the perfusion. The possible explanation could be influenced by the leakage of the contrast agent and the vascular permeability. DCE is influenced by T1 effects of extravasated contrast agents into the interstitial space, while the labeled water proton in the arterial blood acts as a diffusible tracer in ASL, which is less affected by a disrupted BBB [32].

Our study has some limitations: First, this was a retrospective study with a small cohort. A larger number of patients would validate our results in the future. Secondly, it is reported that several factors, including MR sequence parameters, post-processing software, T1 measurement methods, contrast agent may influence on the results.

5. Conclusion

CBF derived from ASL perfusion MRI, V_e and K^{trans} derived from DCE MRI could differentiate PCNSL from HGG and brain metastasis noninvasively. The combination of rCBF and K^{trans} could improve the diagnostic efficiency.

Funding

This work was supported by the National Natural Science Foundation of China (Grants number 81400952 and 81372457).

Appendix A. Supplementary data

Supplementary material related to this article can be found, in the online version, at doi:https://doi.org/10.1016/j.ejrad.2019.01.008.

References

[1] J. Furtner, V. Schopf, M. Preusser, U. Asenbaum, R. Woitek, A. Wohrer, J.A. Hainfellner, S. Wolfsberger, D. Prayer, Non-invasive assessment of intratumoral vascularity using arterial spin labeling: a comparison to susceptibility-weighted imaging for the differentiation of primary cerebral lymphoma and glioblastoma, Eur. J. Radiol. 83 (5) (2014) 806–810.

[2] Y. Ding, Z. Xing, B. Liu, X. Lin, D. Cao, Differentiation of primary central nervous system lymphoma from high-grade glioma and brain metastases using susceptibility-weighted imaging, Brain Behav. 4 (6) (2014) 841–849.

[3] S. Lu, Q. Gao, J. Yu, Y. Li, P. Cao, H. Shi, X. Hong, Utility of dynamic contrast-enhanced magnetic resonance imaging for differentiating glioblastoma, primary central nervous system lymphoma and brain metastatic tumor, Eur. J. Radiol. 85 (10) (2016) 1722–1727.

[4] P. Kickingereder, B. Wiestler, F. Sahm, S. Heiland, M. Roethke, H.P. Schlemmer, W. Wick, M. Bendszus, A. Radbruch, Primary central nervous system lymphoma and atypical glioblastoma: multiparametric differentiation by using diffusion-, perfusion-, and susceptibility-weighted MR imaging, Radiology 272 (3) (2014) 843–850.

[5] P. Kickingereder, F. Sahm, B. Wiestler, M. Roethke, S. Heiland, H.P. Schlemmer, W. Wick, A. von Deimling, M. Bendszus, A. Radbruch, Evaluation of microvascular permeability with dynamic contrast-enhanced MRI for the differentiation of primary CNS lymphoma and glioblastoma: radiologic-pathologic correlation, AJNR Am. J. Neuroradiol. 35 (8) (2014) 1503–1508.

[6] S. Wang, S. Kim, S. Chawla, R.L. Wolf, D.E. Knipp, A. Vossough, D.M. O'Rourke, K.D. Judy, H. Poptani, E.R. Melhem, Differentiation between glioblastomas, solitary brain metastases, and primary cerebral lymphomas using diffusion tensor and dynamic susceptibility contrast-enhanced MR imaging, AJNR Am. J. Neuroradiol. 32 (3) (2011) 507–514.

[7] S. Lu, S. Wang, Q. Gao, M. Zhou, Y. Li, P. Cao, X. Hong, H. Shi, Quantitative evaluation of diffusion and dynamic contrast-enhanced magnetic resonance imaging for differentiation between primary central nervous system lymphoma and glioblastoma, J. Comput. Assist. Tomogr. 41 (6) (2017) 898–903.

[8] K.K. Jain, P. Sahoo, R. Tyagi, A. Mehta, R. Patir, S. Vaishya, N. Prakash, N. Vasudev, R.K. Gupta, Prospective glioma grading using single-dose dynamic contrast-enhanced perfusion MRI, Clin. Radiol. 70 (10) (2015) 1128–1135.

[9] C. Brendle, J.M. Hempel, J. Schittenhelm, M. Skardelly, G. Tabatabai, B. Bender, U. Ernemann, U. Klose, Glioma grading and determination of IDH mutation status and ATRX loss by DCE and ASL perfusion, Clin. Neuroradiol. 28 (Sep. (3)) (2018) 421–428, https://doi.org/10.1007/s00062-017-0590-z Epub 2017 May 9.

[10] P. Wang, J. Li, Q. Diao, Y. Lin, J. Zhang, L. Li, G. Yang, X. Fang, X. Li, Y. Chen, L. Zheng, G. Lu, Assessment of glioma response to radiotherapy using 3D pulsed-continuous arterial spin labeling and 3D segmented volume, Eur. J. Radiol. 85 (11) (2016) 1987–1992.

[11] J. Zhao, Z.Y. Yang, B.N. Luo, J.Y. Yang, J.P. Chu, Quantitative evaluation of diffusion and dynamic contrast-enhanced MR in tumor parenchyma and peritumoral area for distinction of brain tumors, PLoS One 10 (9) (2015) e0138573.

[12] T. Abe, Y. Mizobuchi, K. Nakajima, Y. Otomi, S. Irahara, Y. Obama, M. Majigsuren, D. Khashbat, T. Kageji, S. Nagahiro, M. Harada, Diagnosis of brain tumors using dynamic contrast-enhanced perfusion imaging with a short acquisition time, Springer Plus 4 (2015) 88.

[13] T. Abe, Y. Mizobuchi, W. Sako, S. Irahara, Y. Otomi, Y. Obama, K. Nakajima, D. Khashbat, M. Majigsuren, T. Kageji, S. Nagahiro, M. Harada, Clinical significance of discrepancy between arterial spin labeling images and contrast-enhanced images in the diagnosis of brain tumors, Magn. Reson. Med. Sci. 14 (4) (2015) 313–319.

[14] P.E. Shrout, J.L. Fleiss, Intraclass correlations: uses in assessing rater reliability, Psychol. Bull. 86 (2) (1979) 420–428.

[15] I.S. Haldorsen, A. Espeland, E.M. Larsson, Central nervous system lymphoma: characteristic findings on traditional and advanced imaging, AJNR Am. J. Neuroradiol. 32 (6) (2011) 984–992.

[16] I.H. Lee, S.T. Kim, H.J. Kim, K.H. Kim, P. Jeon, H.S. Byun, Analysis of perfusion weighted image of CNS lymphoma, Eur. J. Radiol. 76 (1) (2010) 48–51.

[17] K. Yamashita, T. Yoshiura, A. Hiwatashi, O. Togao, K. Yoshimoto, S.O. Suzuki, K. Abe, K. Kikuchi, Y. Maruoka, M. Mizoguchi, T. Iwaki, H. Honda, Differentiating primary CNS lymphoma from glioblastoma multiforme: assessment using arterial spin labeling, diffusion-weighted imaging, and (1)(8)F-fluorodeoxyglucose positron emission tomography, Neuroradiology 55 (2) (2013) 135–143.

[18] T. Noguchi, T. Yoshiura, A. Hiwatashi, O. Togao, K. Yamashita, E. Nagao, T. Shono, M. Mizoguchi, S. Nagata, T. Sasaki, S.O. Suzuki, T. Iwaki, K. Kobayashi, F. Mihara, H. Honda, Perfusion imaging of brain tumors using arterial spin-labeling: correlation with histopathologic vascular density, AJNR Am. J. Neuroradiol. 29 (4) (2008) 688–693.

[19] M. Essig, M.S. Shiroishi, T.B. Nguyen, M. Saake, J.M. Provenzale, D. Enterline, N. Anzalone, A. Dorfler, A. Rovira, M. Wintermark, M. Law, Perfusion MRI: the five most frequently asked technical questions, AJR Am. J. Roentgenol. 200 (1) (2013) 24–34.

[20] M. Bergamino, L. Bonzano, F. Levrero, G.L. Mancardi, L. Roccatagliata, A review of technical aspects of T1-weighted dynamic contrast-enhanced magnetic resonance imaging (DCE-MRI) in human brain tumors, Phys. Med. 30 (6) (2014) 635–643.

[21] P.C. Warnke, J. Timmer, C.B. Ostertag, K. Kopitzki, Capillary physiology and drug delivery in central nervous system lymphomas, Ann. Neurol. 57 (1) (2005) 136–139.

[22] P.P. Molnar, B.P. O'Neill, B.W. Scheithauer, D.R. Groothuis, The blood-brain barrier in primary CNS lymphomas: ultrastructural evidence of endothelial cell death, Neurooncology 1 (2) (1999) 89–100.

[23] X. Lin, M. Lee, O. Buck, K.M. Woo, Z. Zhang, V. Hatzoglou, A. Omuro, J. Arevalo-Perez, A.A. Thomas, J. Huse, K. Peck, A.I. Holodny, R.J. Young, Diagnostic accuracy of T1-Weighted dynamic contrast-enhanced-MRI and DWI-ADC for differentiation of glioblastoma and primary CNS lymphoma, AJNR Am. J. Neuroradiol. 38 (3) (2017) 485–491.

[24] G. Johnson, S.G. Wetzel, S. Cha, J. Babb, P.S. Tofts, Measuring blood volume and vascular transfer constant from dynamic, T(2)*-weighted contrast-enhanced MRI, Magn. Reson. Med. 51 (5) (2004) 961–968.

[25] L. Sunwoo, T.J. Yun, S.H. You, R.E. Yoo, K.M. Kang, S.H. Choi, J.H. Kim, C.H. Sohn, S.W. Park, C. Jung, C.K. Park, Differentiation of glioblastoma from brain metastasis: qualitative and quantitative analysis using arterial spin labeling MR imaging, PLoS One 11 (11) (2016) e0166662.

[26] A. Server, T.E. Orheim, B.A. Graff, R. Josefsen, T. Kumar, P.H. Nakstad, Diagnostic examination performance by using microvascular leakage, cerebral blood volume, and blood flow derived from 3-T dynamic susceptibility-weighted contrast-enhanced perfusion MR imaging in the differentiation of glioblastoma multiforme and brain metastasis, Neuroradiology 53 (5) (2011) 319–330.

[27] M.A. Weber, S. Zoubaa, M. Schlieter, E. Juttler, H.B. Huttner, K. Geletneky, C. Ittrich, M.P. Lichy, A. Kroll, J. Debus, F.L. Giesel, M. Hartmann, M. Essig, Diagnostic performance of spectroscopic and perfusion MRI for distinction of brain tumors, Neurology 66 (12) (2006) 1899–1906.

[28] L. Ludemann, W. Grieger, R. Wurm, P. Wust, C. Zimmer, Quantitative measurement of leakage volume and permeability in gliomas, meningiomas and brain metastases with dynamic contrast-enhanced MRI, Magn. Reson. Imaging 23 (8) (2005) 833–841.

[29] C.C. Ko, M.H. Tai, C.F. Li, T.Y. Chen, J.H. Chen, G. Shu, Y.T. Kuo, Y.C. Lee, Differentiation between glioblastoma multiforme and primary cerebral lymphoma: additional benefits of quantitative diffusion-weighted MR imaging, PLoS One 11 (9) (2016) e0162565.

[30] Y.S. Choi, H.J. Lee, S.S. Ahn, J.H. Chang, S.G. Kang, E.H. Kim, S.H. Kim, S.K. Lee, Primary central nervous system lymphoma and atypical glioblastoma: differentiation using the initial area under the curve derived from dynamic contrast-enhanced MR and the apparent diffusion coefficient, Eur. Radiol. 27 (4) (2017) 1344–1351.

[31] A.H. Bauer, W. Erly, F.G. Moser, M. Maya, K. Nael, Differentiation of solitary brain metastasis from glioblastoma multiforme: a predictive multiparametric approach using combined MR diffusion and perfusion, Neuroradiology 57 (7) (2015) 697–703.

[32] C. Warmuth, M. Gunther, C. Zimmer, Quantification of blood flow in brain tumors: comparison of arterial spin labeling and dynamic susceptibility-weighted contrast-enhanced MR imaging, Radiology 228 (2) (2003) 523–532.